Journal of Molecular Structure 1012 (2012) 168–176

Contents lists available at SciVerse ScienceDirect

Journal of Molecular Structure

journal homepage: www.elsevier.com/locate/molstruc

Vibrational spectral and quantum chemical investigations of tert-butyl-hydroquinone

Ö. Dereli [a,*], Y. Erdogdu [b], M.T. Gulluoglu [b], E. Türkkan [a], A. Özmen [c], N. Sundaraganesan [d]

[a] A. Keleşoğlu Education Faculty, Department of Physics, Konya University, Meram, 42090 Konya, Turkey
[b] Department of Physics, Ahi Evran University, 40040 Kirsehir, Turkey
[c] Science Faculty, Department of Physics, Selcuk University, Selcuklu, 42079 Konya, Turkey
[d] Department of Physics (Engg.), Annamalai University, Annamalai Nagar, Chidambaram 608 002, Tamil Nadu, India

ARTICLE INFO

Article history:
Received 30 October 2011
Received in revised form 19 December 2011
Accepted 3 January 2012
Available online 9 January 2012

Keywords:
Tert-butyl-hydroquinone
B3LYP
TD-DFT
FT-IR
Micro-Raman
UV–visible

ABSTRACT

The Fourier transform infrared (FT-IR) and micro-Raman spectra of tert-butyl-hydroquinone were recorded in the region 4000–400 cm^{-1} and 4000–50 cm^{-1}, respectively. Conformational space was scanned with molecular mechanic simulations. All other calculations were performed by B3LYP/6-311G++(d,p) level of theory. The molecular structure and vibrational frequencies of the title compound were calculated and compared with experimental spectra. Theoretical vibrational spectra of the title compound were interpreted by means of TEDs. Predicted electronic absorption spectrum of tert-butyl-hydroquinone from TD-DFT calculation was analyzed and compared with the experimental UV–visible spectrum.

1. Introduction

It is known that quinone derivatives especially hydroquinone and its certain derivatives are capable of inhibiting free-radical fragmentation reactions which play an essential role in the damage of biologically important molecules [1–3]. Because they are found as structural units in a great variety of natural compounds showing antifungal, antibacterial, antiviral and anticancer activity, quinone derivatives are valuable intermediates for the preparation of fine chemicals and pharmaceuticals [4–7]. Tert-butyl-hydroquinone (TBHQ), an important derivative of quinones, is a highly effective and general purpose antioxidant used to preserve various oils, fats and food items by retarding their oxidative deterioration [8,9]. Since it is helpful to skin repairing and the cell renewing, TBHQ is also used to prevent oxidation degradation of cosmetics [10,11].

We have studied molecular structure and vibrational spectra of similar molecules recently [12–14]. The experimental and theoretical vibrational spectrum and assignments or structural studies of TBHQ have not been reported so far.

In the present work, an exhaustive conformational search of the TBHQ has been performed. Vibrational frequencies and molecular structure parameters of the title compound have been calculated by B3LYP/6-311++G(d,p) level of theory. The calculated molecular structure parameters and vibrational frequencies have been analyzed and compared with obtained experimental datas. In addition, HOMO, LUMO and UV spectral analysis have been used to elucidate the information regarding charge transfer within the molecule.

2. Experimental

The sample TBHQ in the powder form was purchased from Sigma–Aldrich Chemical Company. IR measurement of TBHQ molecule at room temperature was recorded by using a Perkin Elmer Spectrum One FT–IR spectrometer in the region 400–4000 cm^{-1} with a resolution of 2 cm^{-1}. The sample was compressed into self-supporting pellet and introduced into an IR cell equipped with KBr window. On the other hand, the Raman spectrum of TBHQ molecule was recorded with a Jasco NRS-3100 micro-Raman Spectrophotometer (1200 lines/mm grating and high sensitivy cooled CCD) at room temperature in the region 50–4000 cm^{-1}. The sample was excited by using 785 nm diode laser. The spectrometer was calibrated with the silicon phonon mode at 520 cm^{-1} and microscope objective 100× was used. Over 50 spectra were taken at an exposure time of 30 s. The measured and calculated FT-IR and micro-Raman spectra are shown in Figs. 1 and 2.

* Corresponding author. Tel.: +90 533 556 9111; fax: +90 332 323 8225.
E-mail address: odereli@selcuk.edu.tr (Ö. Dereli).

0022-2860/$ - see front matter © 2012 Elsevier B.V. All rights reserved.
doi:10.1016/j.molstruc.2012.01.003

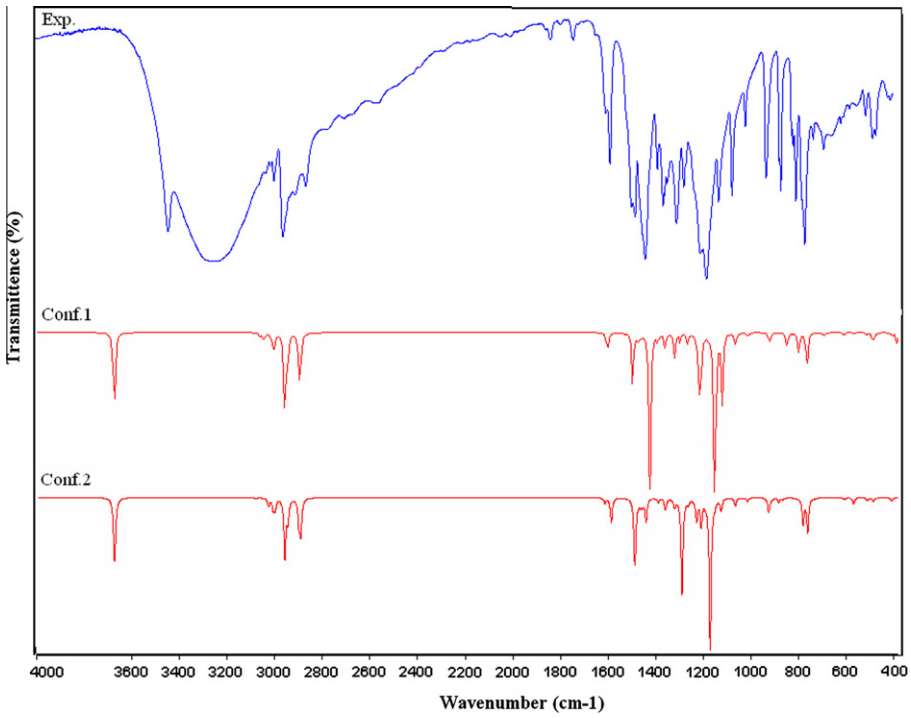

Fig. 1. Experimental and theoretical IR spectra of TBHQ.

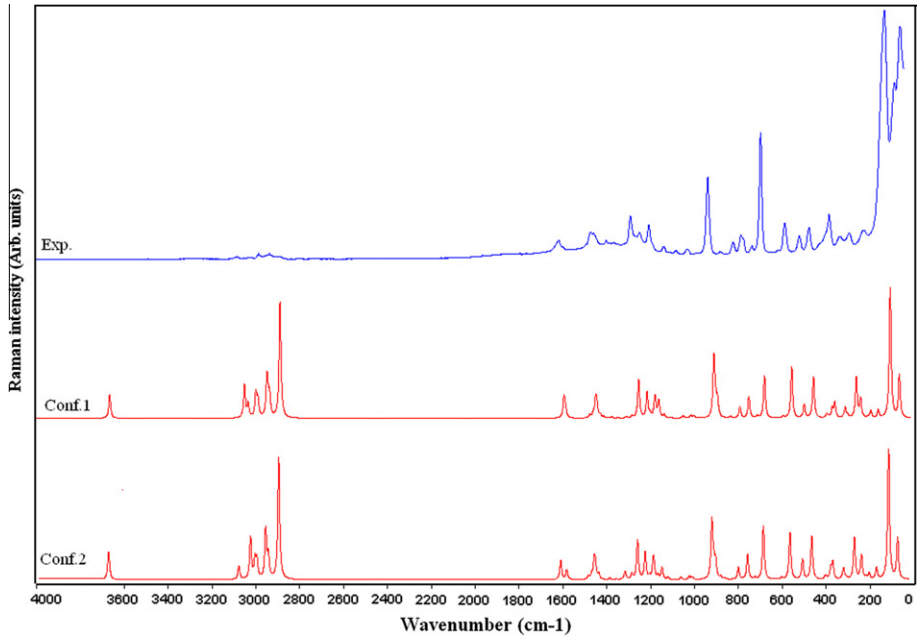

Fig. 2. Experimental and theoretical Raman spectra of TBHQ.

3. Computational details

In order to establish stable possible conformations, the conformational space of TBHQ was scanned with molecular mechanics method. This calculation was performed with the Spartan 08 program [15]. Then, geometry optimizations of the obtained possible conformations were performed with B3LYP/6-311++G(d,p) level of theory. After the most stable conformer of the title compound was determined, geometry optimizations and frequency calculations of this conformer were performed by B3LYP/6-311++G(d,p) level of theory. The optimized structural parameters were used in the vibrational frequency calculations at the same level to characterize all stationary points as minima. In this step, all the calculations were performed using Gaussian 03W program package [16] with the default convergence criteria without any constraint on the geometry [17]. The theoretical vibrational spectra of the title compound were interpreted by means of TEDs using the SQM program [18]. It should be noted that Gaussian 03 package does not calculate the Raman intensities. The Raman activities were transformed into Raman intensities by using Raint program [19].

4. Results and discussion

4.1. Conformational stability

The different conformational structures of a compound are correlated with many of the physical and chemical properties. Hence, their investigation is important for drug designs and to understand several medicinal effects. To found stable conformers, a meticulous conformational analysis was carried out for the title compound. Rotating 10° each degree intervals around the free rotation bonds, conformational space of the title compound was scanned by molecular mechanic calculation. The geometry optimizations of the obtained conformers were performed by B3LYP/6-311++G(d,p) level of theory. Results of conformational analysis indicated that the title compound has eight conformers as shown in Fig. 3. The molecular structure with atom numbering scheme for conformer is given in Fig. 4. In all cases, given in Fig. 3 trans orientations of the hydroxyl groups are favored. At first glance, the main reason of the energy distribution seems to be the tert-butyl group orientation relative to the nearest hydroxyl group. For this reason, we investigated whether the most stable structure 1 result from formation of C–H···O contact (hydrogen bonding-like interaction) or not. Because the calculated C–H···O distances are approximately 2.4 Å, we have concluded that hydrogen bonding-like interactions does not responsible for stability of conformer 1 but long-range electrostatic interactions can be responsible for it due to the fact that it was observed at one of our previous study [20].

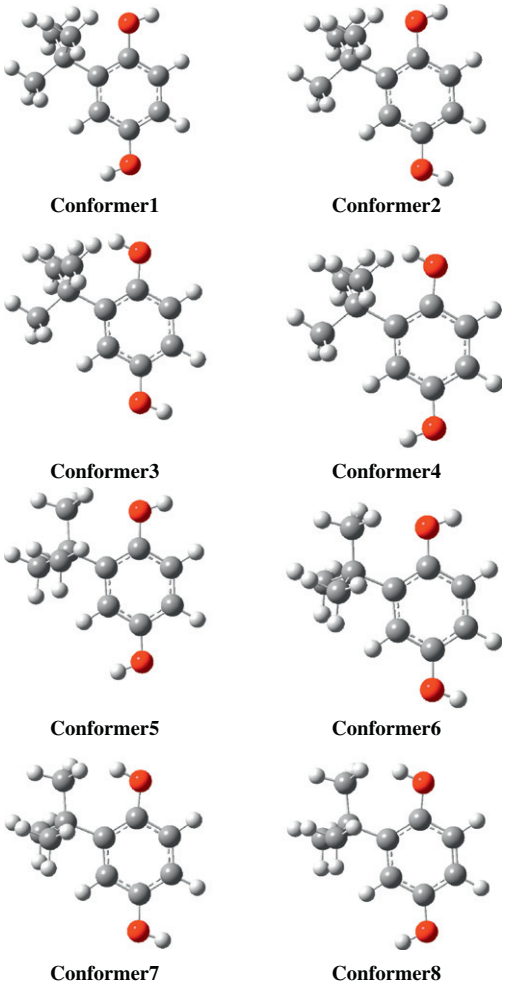

Fig. 3. Stable conformers of TBHQ.

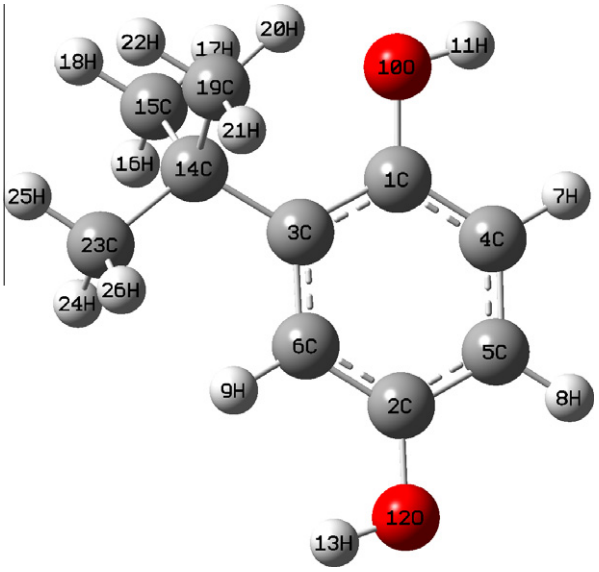

Fig. 4. Molecular structure and atom numbering scheme adopted in this study for TBHQ.

Ground state energies, zero point corrected energies (E_{elect} + ZPE), relative energies of conformers and dipole moments, were presented in Table 1. From the calculated energies of eight conformers, given in Table 1, the conformer 1 is the most stable. Zero point corrections have not caused any significant changes in the stability order.

The difference between the total energies of the most stable two conformers is 0.301 kJ/mol for total energies and 0.157 kJ/mol for zero point corrected energies. The only difference between molecular structures of these two conformers is in the orientation of H_{13} atom. A detailed potential energy surface (PES) scan in C_6–C_2–O_{12}–H_{13} dihedral angle was performed. This scan was carried out by relaxed PES scanning calculations in all geometrical parameters by changing the torsion angle for every 10° rotation around the bond. The shape of the potential energy as a function of the dihedral angle is illustrated in Fig. 5. As seen in Fig. 5, the conformer 1 with a zero degree C_6–C_2–O_{12}–H_{13} dihedral angle is the most stable conformer. Optimized energy of the conformer 2 is slightly larger than those of conformer 1. Therefore, both forms were used in the future calculations such as molecular structure, vibrational and UV–visible and molecular electrostatic potential analysis of the title molecule.

4.2. Molecular geometry

The optimized geometric parameters (bond lengths, bond angles and dihedral angles) of the conformer 1 and conformer 2 were given in Table 2. In the literature, we have found neither experimental data nor the calculation results on molecular structure of TBHQ, therefore the molecular structure of conformer 1 and conformer 2 was compared with XRD data of closely related molecule like 2,6-di-tert-butylphenol [21].

For the most stable conformer, two hydroxyl groups are planar and lies in the same plane of the benzene ring moiety which can be seen from the torsion angle value of C_3–C_1–O_{10}–H_{11} = 180° and C_5–C_2–O_{12}–H_{13} = 180°. The optimized geometry shows that two of the CH_3 groups $C_{15}H_3$ and $C_{19}H_3$ substituted in ortho position of phenyl ring are out-of-plane as evident from the dihedral angles C_1–C_3–C_{14}–C_{15} = 60.6°, C_1–C_3–C_{14}–C_{19} = 60.6°. The optimized geometry

Table 1
Energetics of the conformers calculated at the B3LYP/6-311++G(d,p) level.

Conformers	E (Hartree)	ΔE (kJ/mol)	E_0 (Hartree)	ΔE_0 (kJ/mol)	Dip. mom. (D)
1	−540.096910	0.000	−539.876901	0.000	0.43
2	−540.096795	0.301	−539.876841	0.157	2.51
3	−540.093818	8.118	−539.874153	7.214	0.66
4	−540.093402	9.210	−539.873722	8.346	3.33
5	−540.091251	14.85	−539.871588	13.94	0.33
6	−540.091184	15.03	−539.871502	14.17	2.46
7	−540.090617	16.52	−539.870758	16.12	0.84
8	−540.090147	17.75	−539.870337	17.23	3.48

E_0, zero point corrected energy.

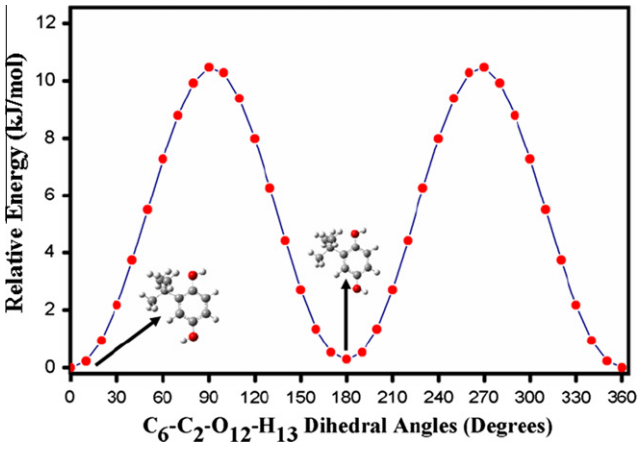

Fig. 5. Potantial energy surface scan.

also shows that two carbon atoms (C_{14} and C_{23}) are in the plane of the ring as evident from the torsional angles C_1–C_3–C_{14}–C_{23} = 180°. The small differences between experimental and calculated geometrical parameters may come from the environment of the compound. It is clear that the experimental results belong to solid phase while theoretical calculations belong to gaseous phase.

4.3. Vibrational assignments

The TBHQ molecule has 26 atoms, which possess 72 normal modes of vibrations. All the vibrations are active in the infrared and Raman spectra. Usually the calculated harmonic vibrational wavenumbers are higher than the experimental ones, because of the anharmonicity of the incomplete treatment of electron correlation and of the use of finite one-particle basis set. The harmonic frequencies were calculated by B3LYP/6-311++G(d,p) level of theory and then scaled by 0.967 for wave numbers under 1800 cm^{-1} and 0.955 for those over 1800 cm^{-1}. In order to correct the overestimations of the calculated harmonic wavenumbers, three different scaling procedures referred to as scaling procedure-1: "scaling wavenumbers with dual scale factors [22]" and scaling procedure-2: "Scaled Quantum Mechanics Force Field (SQM FF) methodology [18,23,24]" or scaling procedure-3: single scaling factors, were performed independently. It can be seen that the calculated results with dual scaling is better than single scaling and SQM method resulted in the best agreement with the experimental wavenumbers [25]. In this study, we have used the first method. Experimentally observed and theoretically calculated harmonic vibrational frequencies and their correlations were gathered in Table 3. From the calculations, the computed values are in good agreement with the observed values. The vibrational bands assignments have been made by using the animation option of Gauss View 3.0 graphical interface for Gaussian programs [26] along with available related molecules and also by means of TEDs using the SQM program [18].

4.3.1. O–H vibrations

The O–H group gives rise to the three vibrations viz., stretching, in-plane bending and out-of-plane bending vibrations. The O–H group vibrations are likely to be the most sensitive to the environment, so they show pronounced shifts in the spectra of the hydrogen-bonded species. In the case of unsubstituted phenol it has been shown that the frequency of O–H stretching vibration in the gas phase is 3657 cm^{-1} [27]. In our previous study of 2,5-di-tert-butylhydroquinone [13], a strong band in FT-IR spectrum at 3402 cm^{-1} was assigned to O–H stretching vibration. In the FT-IR spectrum of title compound, the band observed at 3445 cm^{-1} is assigned to O–H stretching mode. The theoretically computed and scaled value of O–H band is 3669 cm^{-1} (mode no. 1). In addition to this, as it is seen in Table 3, the theoretically computed wavenumber of mode no. 2, which was calculated as 3667 cm^{-1}, is another O–H stretching vibration of the title compound. A comparison of these bands with experimental data predicts that there are negative deviations owning to the fact that the presence of strong intermolecular hydrogen bonding. In general, for phenols the in-plane bending vibrations lies in the 1150–1250 cm^{-1} region [27]. The band observed at 1183 cm^{-1} and the band observed at 1133 cm^{-1} in FT-IR spectrum were assigned to OH in-plane bending vibration (mode nos: 35 and 36). The same vibration was observed in FT-Raman spectrum as a weak band at 1133 cm^{-1}. The theoretically computed values of these bands are 1165 and 1141 cm^{-1}, respectively. These vibrations were observed at 1190 and 1118 cm^{-1} in FT-IR spectrum of 2,5-di-tert-butylhydroquinone [13] In this study, the scaled values of OH out-of-plane bending vibrations are 264 and 265 cm^{-1} (mode nos: 64 and 65).

4.3.2. C–H vibrations

The aromatic CH stretching vibrations of heteroaromatic structures are expected to appear in the 3100–3000 cm^{-1} frequency ranges, with multiple weak bands. The nature of substituents cannot affect the bands much in this region [27,28]. The CH in-plane bending vibrations appear by sharp but weak to medium intensity bands in the 1100–1500 cm^{-1} region. These bands are not sensitive to the nature of substituents [28]. The out-of-plane bending vibrations occur in the wavenumber range 800–1000 cm^{-1} [28].

The aromatic CH stretching vibrations of the title compound were observed as very weak bands at 3067, 3035 and 3016 cm^{-1} in the FT-IR spectrum (mode nos. 3–5). In the FT-Raman spectrum, these vibrations were observed at 3064 and 3031 cm^{-1}. The theoretically computed wavenumbers at 3054, 3037 and 3002 cm^{-1} were well correlated with the experimental values. The in-plane CH bending vibration was observed at 1310 cm^{-1} in FT-IR spectrum (mode no. 29). According to the TED analysis given in Table 3, the theoretically computed harmonic wavenumber of mode no 37 was assigned to the another in-plane CH bending vibration. The bands observed at 820 and 771 cm^{-1} in the FT-IR spectrum, the bands observed at 820 and 774 cm^{-1} in the Raman spectrum (mode nos. 46, 48) and the theoretically calculated value of mode no 45 were assigned to out-of-plane CH vibrations. These results were found to be in the same range as in literature [29–32]. The calculated wavenumbers of in-plane and out-of-plane CH bands were well reproduced the experimental ones in the infrared and Raman spectra.

4.3.3. Tert-butyl group vibrations

Isopropyl and tertiary butyl groups give characteristic doublets in the symmetric CH3 bending region of the IR spectrum. The tert

Table 2
The calculated geometric parameters of tert-butyl-hydroquinone by B3LYP/6-311++G(d,p)method, bond lengths in angstrom (Å) and angles in degrees (°).

Parameters	Calculated		Experimental[a]	Parameters	Calculated		Experimental[a]
	Conformer1	Conformer 2			Conformer1	Conformer 2	
Bond lengths (Å)				*Bond angles (°)*			
C_1–C_3	1.409	1.413	1.415	C_6–C_3–C_{14}	121.4	121.3	121.0
C_1–C_4	1.394	1.391	1.414	C_1–C_4–C_5	121.5	121.3	121.6
C_1–O_{10}	1.381	1.381	1.386	C_2–C_5–C_4	118.6	118.8	116.8
O_{10}–H_{11}	0.962	0.962	0.846	C_2–C_6–C_3	122.8	122.7	121.6
O_{12}–H_{13}	0.962	0.962	–	C_3–C_{14}–C_{15}	109.9	109.9	110.0
C_2–C_5	1.389	1.389	1.386	C_3–C_{14}–C_{19}	109.9	109.9	110.4
C_2–C_6	1.395	1.395	1.391	C_3–C_{14}–C_{23}	112.0	111.9	111.8
C_2–O_{12}	1.375	1.376	–	C_{15}–C_{14}–C_{19}	110.0	110.0	110.4
C_3–C_6	1.401	1.397	1.395	C_{15}–C_{14}–C_{23}	107.5	107.5	106.9
C_3–C_{14}	1.542	1.542	1.545	C_{19}–C_{14}–C_{23}	107.5	107.5	107.3
C_4–C_5	1.390	1.394	1.400	*Selected dihedral angles (°)*			
C_{14}–C_{15}	1.548	1.548	1.544	O_{10}–C_1–C_3–C_6	180.0	180.0	178.3
C_{14}–C_{19}	1.548	1.548	1.544	O_{10}–C_1–C_3–C_{14}	0.0	0.0	1.441
C_{14}–C_{23}	1.541	1.541	1.539	O_{12}–C_2–C_5–C_4	180.0	180.0	–
Bond angles (°)				O_{12}–C_2–C_6–C_3	180.0	180.0	–
C_3–C_1–C_4	120.9	120.9	122.9	C_1–C_3–C_{14}–C_{15}	60.6	60.6	61.5
C_3–C_1–O_{10}	119.1	119.1	116.5	C_1–C_3–C_{14}–C_{19}	60.6	60.6	60.6
C_4–C_1–O_{10}	120.0	120.1	120.6	C_1–C_3–C_{14}–C_{23}	180.0	180.0	179.7
C_5–C_2–C_6	119.8	119.8	–	C_6–C_3–C_{14}–C_{15}	119.4	119.4	118.2
C_5–C_2–O_{12}	117.8	123.5	–	C_6–C_3–C_{14}–C_{19}	119.4	119.4	119.7
C_6–C_2–O_{12}	122.4	117.0	–	C_6–C_3–C_{14}–C_{23}	0.0	0.0	0.7
C_1–C_3–C_6	116.4	116.6	116.9	C_3–C_1–O_{10}–H_{11}	180.0	180.0	179.2
C_1–C_3–C_{14}	122.2	122.2	122.0	C_5–C_2–O_{12}–H_{13}	180.0	0.0	–

[a] X-ray data taken from closely related molecule like 2,6 di-tert-butylphenol. Ref. [21].

Table 3
Comparison of the observed and calculated vibrational spectra of TBHQ.

Mode nos.	Experimental		Theoretical						TED[d] (%)
	IR	RAMAN	Conformer 1			Conformer 2			
			Scaled Freq[a]	I^b_{IR}	I^c_{RAMAN}	Scaled Freq[a]	I^b_{IR}	I^c_{RAMAN}	
ν_1	3445 m	–	3669	8	14	3670	24	14	96 υ_s OH
ν_2	–	–	3667	37	4	3667	22	9	96 υ_a OH
ν_3	3067 vw	3064 m	3054	2	25	3075	1	10	98 υ_sCH,ring
ν_4	3035 vw	3031 m	3037	4	10	3021	5	31	99 υ_aCH,ring
ν_5	3016 w	–	3002	7	18	3001	8	14	98 υ_sCH,ring
ν_6	3002 w	3002 w	2993	7	12	2992	7	12	99 υ_a (CH_3),tb
ν_7	–	–	2991	0	2	2990	0	2	94 υ_s (CH_3),tb
ν_8	2962 s	2965 s	2952	26	27	2952	25	27	97 υ_a (CH_3),tb
ν_9	–	–	2948	16	10	2952	14	10	92 υ_a (CH_3),tb
ν_{10}	–	–	2940	10	14	2940	9	14	97 υ_s (CH_3),tb
ν_{11}	–		2938	4	3	2938	5	3	91 υ_a (CH_3),tb
ν_{12}	2911 w	2917 s	2892	17	88	2893	16	88	97 υ_s (CH_3),tb
ν_{13}	–	–	2885	15	1	2886	8	3	97 υ_a (CH_3),tb
ν_{14}	2867w	2871w	2884	9	2	2885	14	1	95 υ_s (CH_3),tb
ν_{15}	1608 w	1608 m	1597	5	17	1605	3	14	68 υ CC, ring + 11 δ HCC
ν_{16}	1590 s	1591 vw	1590	7	6	1579	16	7	58 υ CC, ring + 14 δ CCC
ν_{17}	1498 w	–	1489	23	0	1480	22	1	42 υ CC, ring + 19 δ HCC
ν_{18}	1484 w	–	1479	5	2	1478	24	1	87 δ_d (CH_3),tb
ν_{19}	–	1463 m	1464	3	3	1464	2	3	82 δ_d (CH_3),tb
ν_{20}	1454 vw	1452 vw	1454	2	13	1453	5	13	80 δ_d (CH_3),tb
ν_{21}	–	–	1448	0	10	1448	0	10	90 δ_d (CH_3),tb
ν_{22}	–	–	1445	0	1	1444	2	1	87 δ_d (CH_3),tb
ν_{23}	1441 vs	–	1431	0	3	1433	15	2	87 δ_d (CH_3),tb
ν_{24}	–	–	1416	81	1	1431	0	2	39 υ CC, ring + 11δ HCC
ν_{25}	1390 w	1393 w	1381	6	1	1382	3	1	87 δ_S (CH_3),tb
ν_{26}	1367 m	–	1351	3	0	1352	4	0	94 δ_S (CH_3),tb
ν_{27}	1360 w	1359 w	1349	4	0	1349	4	0	97 δ_S (CH_3),tb
ν_{28}	1349 w	–	1312	11	1	1312	6	6	46 υ CC, ring + 12δ HCC + 15δ HOC
ν_{29}	1310 m	–	1289	4	2	1281	63	4	34δ HCC, ring + 21δHOC + 16 υCC
ν_{30}	1280 m	1284 s	1257	5	29	1255	3	29	55υOC + 12δHCC
ν_{31}	1235 vw	1243 w	1218	6	20	1220	14	20	31 υ CC,tb + 18 υOC
ν_{32}	1210 m		1205	45	3	1201	18	2	41υ OC + 31δ HCC
ν_{33}	–	1200 m	1184	1	8	1184	1	9	30δ CCC + 21υ CC
ν_{34}	–	–	1181	2	10	1181	1	11	46 ρ_s (CH_3),tb + 23υ CC
ν_{35}	1183 vs	–	1165	2	13	1162	100	3	53 δ HOC + 14 δ HCC
ν_{36}	1133 m	1133 w	1141	100	2	1144	3	9	45δ HOC + 22 δ HCC + 20υ CC
ν_{37}	–	–	1112	31	1	1116	8	2	38 δ HCC,ring + 10 υ CC

Table 3 (*continued*)

Mode nos.	Experimental		Theoretical						TED[d] (%)
	IR	RAMAN	Conformer 1			Conformer 2			
			Scaled Freq[a]	I^{b}_{IR}	I^{c}_{RAMAN}	Scaled Freq[a]	I^{b}_{IR}	I^{c}_{RAMAN}	
ν_{38}	1077 s	1078 w	1054	6	2	1056	5	2	53δ CCC,ring breathing + 11δ HCC
ν_{39}	1021 w	1023 w	1019	0	2	1019	0	2	71 ρ_s (CH_3),tb
ν_{40}			1005	2	2	1006	3	2	69 ρ_s (CH_3),tb
ν_{41}	934 s	935 vs	933	0	0	933	0	0	86 ρ_s (CH_3),tb
ν_{42}	–		914	5	45	916	10	43	65 υ CC
ν_{43}	–	–	907	1	12	908	1	11	49 υCC + 33 δ HCC
ν_{44}	872 s	877 w	898	0	10	899	0	13	57 υCC + 26*Γ* HCCC
ν_{45}	–		896	0	3	874	3	2	90 γ (HC).ring
ν_{46}	820 vw	820 w	838	7	1	857	1	1	83 γ (HC).ring
ν_{47}	784 m	784 m	795	0	9	795	0	9	72 υ CC
ν_{48}	771 s	774 vw	789	14	0	771	17	0	83 γ (HC).ring
ν_{49}	735w	734 w	754	19	17	753	22	18	50 δ CCC ring trigonal bending + 18 υ OC
ν_{50}	692 w	–	715	0	2	718	1	2	59 γ (CC),ring + 11 γ (HC).
ν_{51}	657 vw	695 vs	683	2	33	681	0	39	57 δ CCC + 30 υ CC
ν_{52}	610 vw	616 vw	597	1	1	597	2	2	69 γ (CC),ring
ν_{53}	583vw	585 s	559	0	40	559	4	35	34 υ CC + 14 δ CCC + 10 δ CCC
ν_{54}	516 w	520 m	502	1	11	502	2	15	73 γ (CC),ring
ν_{55}	473 m	476 m	476	6	0	477	3	0	68 γ (CC),ring
ν_{56}	–	–	460	0	32	460	0	32	67 δ CCC
ν_{57}	411 vw	416 vw	399	0	3	399	2	2	75 δ CCC
ν_{58}	–	403 vw	391	1	1	392	0	1	79 γ (CC)
ν_{59}	–	385 s	374	5	7	373	0	7	73 δ CCC
ν_{60}	–	–	363	1	12	364	0	12	65 γ (CC)
ν_{61}	–	337 w	325	0	0	323	0	0	67 τ (CH_3)+ 27 τ (CO)
ν_{62}		–	315	3	8	315	1	8	70 δ(CCO)+ 25 δ(CCC)
ν_{63}	–	293 w	303	1	2	303	0	2	68 δ CCC
ν_{64}	–	–	265	0	19	266	0	16	77 γ (OH)
ν_{65}	–	–	264	42	13	265	40	16	70 γ (OH)
ν_{66}	–	–	246	34	14	242	0	1	68 δ CCC
ν_{67}	–	230 m	243	0	1	233	33	18	92 τ (CH_3)
ν_{68}	–	–	213	1	1	213	1	1	87 τ (CH_3)
ν_{69}	–	–	198	0	6	198	1	5	79 δ CCC
ν_{70}	–	–	165	1	6	165	1	9	79 γ (CO)
ν_{71}	–	135 vs	110	0	100	109	1	100	87 τ (CC),tb
ν_{72}	–	66 m	68	0	33	68	0	31	91 τ (CC),tb

ν – stretching, a – antisymmetric, s – symmetric, δ – in-plane bending, γ – out-of-plane bending, τ – torsional, tb. – tert-butyl group.

[a] Obtained from the wave numbers calculated at B3LYP/6-311++G(d,p) using scaling factors 0.967 (for wave numbers under 1800 cm^{-1}) and 0.955 (for those over 1800 cm^{-1}).

[b] Relative absorption intensities normalized with highest peak absorption equal to 100.

[c] Relative Raman intensities normalized with highest peak absorption equal to 100.

[d] Total energy distribution calculated B3LYP/6-311++G(d,p) level of theory. Only contributions ⩾10% are listed.

butyl group gives rise to two CH bending modes, one in the 1395–1385 cm^{-1} region and another one near 1370 cm^{-1}. In the tert-butyl doublet, the longer wavelength is more intense [33] than the shorter wavelength. In the FT-IR spectrum of TBHQ the band observed at 1367 cm^{-1} and the band at 1390 cm^{-1} were assigned to tert-butyl doublet (mode nos. 25, 26). The Raman counterpart of one of this bans was observed at 1393 cm^{-1} in the Raman spectrum. The theoretically computed wavenumbers are the best correlated with the experimental values.

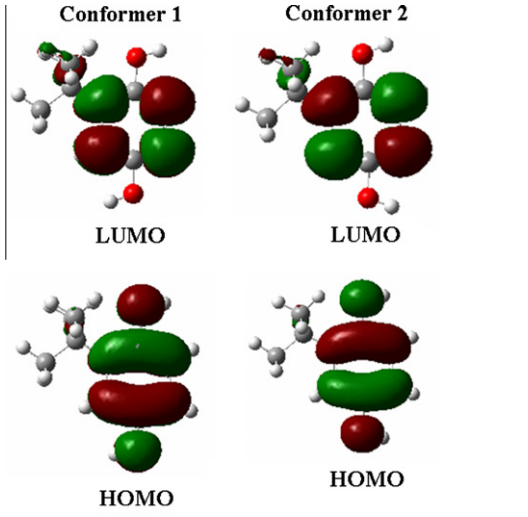

Fig. 6. The atomic orbital compositions of the frontier molecular orbitals for two conformers of TBHQ.

The skeletal C–C vibrations of tert-butyl group appear around 1255 and 1200 cm^{-1}, with medium intensity bands [33]. The band observed at 1235 cm^{-1} in the FT-IR spectrum and the band observed at 1243 cm^{-1} in the Raman spectrum were assigned to skeletal C–C vibrations of tert-butyl group (mode no. 31). The theoretically predicted wavenumber is in good agreement with the observed wavenumber.

For the methyl group vibrations in the tert-butyl group, the bands observed at 3002, 2962 cm^{-1} in FT-IR spectrum and the

Table 4
HOMO–LUMO energies and energy gaps of two conformers of TBHQ.

	HOMO energy (a.u)	LUMO energy (a.u)	HOMO–LUMO energy gap (a.u)
Conformer 1	−0.20934	−0.01721	0.19312
Conformer 2	−0.20942	−0.01699	0.19243

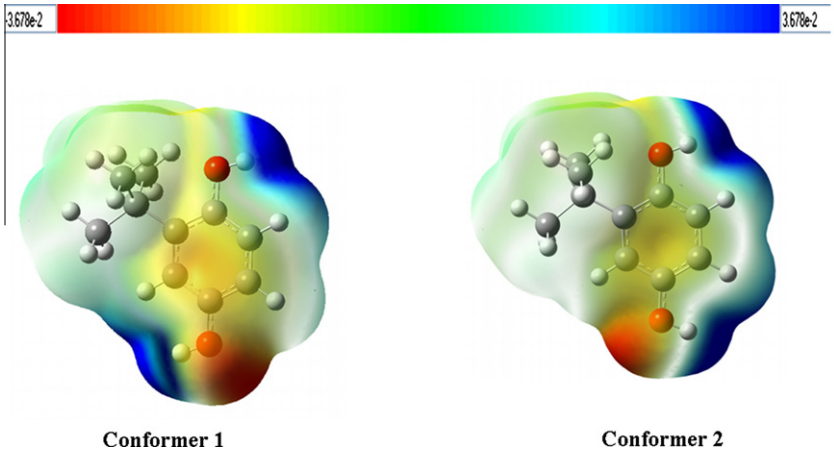

Fig. 7. The electrostatic potential maps for two conformers of THBQ.

bands observed at 3002 and 2965 cm^{-1} in Raman spectrum were assigned to CH_3 antisymmetric stretching vibrations.The CH_3 symmetric stretching vibrations were observed at 2911 and 2867 cm^{-1} in the FT-IR spectrum. In the Raman spectrum, these vibrations were observed at 2917 and 2871 cm^{-1}. The theoretically predicted asymmetric and symmetric CH_3 stretching vibrations show good agreement with the experimental values. The bands observed at 1484, 1454 and 1441 cm^{-1} in the FT-IR spectrum and the bands observed at 1463 and 1452 cm^{-1} in the Raman spectrum were assigned to degenerate bending (mode nos. 18–23); the bands observed at 1390, 1367 and 1360 cm^{-1} in the FT-IR spectrum and the bands observed at 1393 and 1359 cm^{-1} in Raman spectrum were assigned to symmetric bending (mode nos. 25–27); the bands observed at 1021 and 934 cm^{-1} in the FT-IR spectrum and the bands observed at 1023 and 935 cm^{-1} in the Raman spectrum were assigned to rocking vibrations of CH_3 of tert-butyl groups (mode nos. 39,41). The experimental and theoretical wavenumbers of tert-butyl group and CH3 group vibrations show the good correlation with the literature data [12–14].

4.3.4. C–O vibrations

The CO stretching vibrations in phenols are expected to appear as a strong band in the 1300–1200 cm^{-1} frequency ranges [34]. These vibrations were observed at 1265 and 1226 cm^{-1} in FT-Raman spectrum of 2,5-di-tert-butylhydroquinone [13]. In our present work, The bands observed at 1280 and 1210 cm^{-1} in FT-IR spectrum and the band observed at 1284 cm^{-1} in Raman spectrum were assigned to C–O stretching mode of C–OH vibration (mode nos. 30,32), which is in agreement with the literature data [31,13]. In addition to this, the theoretically calculated wavenumbers in this study show good agreement with measured experimental data. In the vibrational studies of some phenols, Sundaraganesan et al. [29] and Subramanian et al. [30] have assigned the frequencies at 326 and 314 cm^{-1} to in-plane C–O bending mode and 221 and 170 cm^{-1} to out-of-plane C–O bending mode of vibration. In our case, the calculated values of in-plane and out-of plane C–O bending modes are at 315 cm^{-1} and 165 cm^{-1} (mode nos. 62 and 70), respectively.

4.3.5. C=C vibrations

The ring carbon–carbon stretching vibration occurs in the region 1625–1430 cm^{-1}. In general, the bands are of variable intensity and are observed at 1625–1590, 1590–1575, 1540–1470, 1460–1430 and 1380–1280 cm^{-1} from the frequency ranges given by Varsanyi [27] for the five bands in the region. In the present work, the frequencies observed in the FT-IR spectrum at 1608, 1590, 1498 and 1349 cm^{-1}, the frequencies observed in Raman spectrum at 1608 and 1591 cm^{-1} and predicted wavenumber at 1416 cm^{-1} were assigned to C–C stretching vibrations (mode nos: 15–17, 24 and 28). The ring breathing mode at 1077 and 1078 cm^{-1} in FT-IR and Raman spectra, respectively coincide with the predicted value at 1054 cm^{-1} (mode no. 38). The predicted wavenumber at 754 cm^{-1} was assigned to trigonal bending mode (mode no. 49). This vibration was observed at 735 and 734 cm^{-1} in our FT-IR and Raman spectra, respectively. The bands at 610, 516 and 473 cm^{-1} in FT-IR spectrum and the bands observed at 616, 520 and 476 cm^{-1} in FT-Raman spectrum were assigned to C–C–C ring out-of-plane bending modes (mode nos. 52, 54, 55).

4.4. Absorption spectra

On the basis of fully optimized ground-state structures of two conformers, TD-DFT//B3LYP/6-311++G(d,p) calculations have been used to determine the low-lying excited states of TBHQ. The calculated results involving the vertical excitation energies, oscillator strength (f) and wavelength of the most stable two conformers were carried out and compared with measured experimental wavelength. Typically, according to Frank–Condon principle, the maximum absorption peak (max) corresponds in an UV–visible spectrum to vertical excitation. TD-DFT//B3LYP/6-311++G(d,p) predict one intense electronic transition at 4.5695 eV (271.33 nm) with an oscillator strength $f = 0.1014$ for conformer 1 and one intense electronic transition at t 4.5749 eV (271.01 nm) with an oscillator strength $f = 0.0995$ for conformer 2. These are in good agreement with the measured experimental data in water solution (exp = 292 nm) [35]. Similar calculations were performed for other solutions that were given in experimental UV–visible study [35] and the results of these calculations were presented in Table S1 (Supplementary information).

This electronic absorption corresponds to the transition from the ground to the first excited state and it is mainly described by one electron excitation from the highest occupied molecular orbital (HOMO) to the lowest unoccupied molecular orbital (LUMO). The atomic orbital compositions of the frontier molecular orbitals of the conformers are sketched in Fig. 6.

The calculated HOMO–LUMO energies and HOMO–LUMO energy gaps, which reflect the chemical activity of the molecule, of conformers are given in Table 4. LUMO as an electron acceptor represents the ability to obtain an electron, HOMO represents the ability to donate an electron. As it is seen in Fig. 6, the HOMO is located over the OH group and phenyl ring and the LUMO located over the phenyl ring, the HOMO → LUMO transition implies an electron

density transfer to ring from OH group. Moreover, these orbitals significantly overlap in their position for TBHQ conformers.

4.5. Molecular electrostatic potential

The Molecular Electrostatic Potential (MEP) is the most useful electrostatic property to study the relation between structure and activity. The MSEP has been also employed as an informative tool of chemistry to describe different physical and chemical features, including non-covalent interactions in complex biological system.

The electrostatic potential created by the nuclei and electrons of a molecule in the surrounding space is well established as a guide to the interpretation and prediction of molecular behavior. It has been shown to be a useful tool in studying both electrophilic and nucleophilic processes, in particular, to be well suited for studies that involve the identification of key features necessary for the "recognition" of one molecule by another. The molecular surface electrostatic potential (MSEP) is rigorously defined as the first order interaction between a positive unit charge at any point in the vicinity of a molecule and its charge distribution contributed by both electrons and nuclei. The potential $V(r)$ can be calculated through the folowing equation:

$$V(r) = \sum_A \frac{Z_A}{|R_A - r|} = \int \frac{\rho(\acute{r})d\acute{r}}{|\acute{r} - r|} \quad (1)$$

where Z_A is the charge on nucleus A; at a distance R_A; and $\rho(r)$ is the electronic density function defined by the 0.001 a.u. contour.

The electron density isosurfaces on which the electrostatic potential surface have been mapped are shown in Fig. 7 for two conformers of title compound. The different values of the electrostatic potential at the surface are represented by different colors[1]; red represents regions of most negative electrostatic potential, blue represents regions of most positive electrostatic potential and green represents regions of zero potential.

As seen in Fig. 7, the positive energy area (blue color) is observed over the H atoms of O_{10}–H_{11} and O_{12}–H_{13} group. The red regions refer to an area that would favor interactions with approaching electrophiles. The blue regions interact extensively with incoming nucleophiles and thus the sites of hydrogen bond donor groups. The red region is the site of hydrogen bonding acceptors (O_{12} atom). O_{10}–H_{11} group is not the site of hydrogen bonding acceptors, due to tert-butyl group [36–39].

5. Conclusion

The FT-IR and FT-Raman spectra were studied. The equilibrium geometries, harmonic wavenumbers and TD/DFT calculations (Conformer 1 and Conformer 2) were carried out for the first time at DFT/B3LYP/6-311++G(d,p) level of theory. Optimized geometrical parameters of the title compound were in agreement with the crystal structure data obtained from XRD studied. B3LYP level of theory with the higher basis set 6-311++G(d,p) calculations showed better correlation with the experimental results. Ab initio programs were used to find the most stable conformer of TBHQ. The theoretical TD-DFT/ B3LYP/6-311++G(d,p) level of calculated results also complemented with measured UV–visible spectral data. The theoretically constructed FT-IR and FT-Raman spectra showed good correlation with experimentally observed FT-IR and FT-Raman spectra.

Acknowledgment

This work was supported by the BAP office of Selcuk University (Project Number: 11401012).

Appendix A. Supplementary material

Supplementary data associated with this article can be found, in the online version, at doi:10.1016/j.molstruc.2012.01.003.

References

[1] N. Cotele, S. Moreau, J.S. Bernier, J.P. Catteau, J.P. Henichart, Free Radic. Biol. Med. 11 (1991) 63.
[2] O.I. Shadyro, G.K. Glushonok, T.G. Glushonok, I.P. Edimechieva, A.G. Moroz, A.A. Sosnovskaya, I.L. Yurkova, G.I. Polozov, Free Radic. Res. 36 (2002) 859.
[3] L.F. Yamaguchi, J.H.G. Lago, T.M. Tanizaki, P.D. Mascio, M.J. Kato, Phytochemistry 67 (2006) 1838.
[4] P. Schudel, H. Mayer, O. Isler, in: W.H. Sebrell, R.S. Harris (Eds.), The Vitamins, vol. 5, Academic Press, New York, 1972, p. 165.
[5] B.H. Lipshutz, P. Mollard, S.S. Pfeiffer, W. Chrisman, J. Am. Chem. Soc. 124 (2002) 14282.
[6] S. Patai (Ed.), The Chemistry of Quinonoid Compounds, Part 2, Wiley, New York, 1988.
[7] R. Maggi, C.G. Piscopo, G. Sartori, L. Storaro, E. Moretti, Appl. Catal. A: Gen., in press. doi:10.1016/j.apcata.2011.10.032 (accepted manuscript).
[8] R.D. O'Brien, Fats and Oils: Formulating and Processing for Applications, CRC Press, 2008.
[9] U.N. Wanasundara, F. Shahidi, Food Chem. 63 (1998) 335.
[10] Y.Q. Guan, Q.C. Chu, L. Fu, J.N. Ye, J. Chromatogr. A 1074 (2005) 201.
[11] B.B. Sha, X.B. Yin, X.H. Zhang, X.W. He, W.L. Yang, J. Chromatogr. A 1167 (2007) 109.
[12] P. Chinna Babu, N. Sundaraganesan, O. Dereli, E. Turkkan, Spectrochim. Acta A: Mol. Biomol. Spectrosc. 79 (2011) 562.
[13] N. Subramanian, N. Sundaraganesan, O. Dereli, E. Turkkan, Spectrochim. Acta A: Mol. Biomol. Spectrosc. 83 (2011) 165–174.
[14] S. Kalaichelvan, N. Sundaraganesan, O. Dereli, U. Sayin, Spectrochim. Acta A: Mol. Biomol, Spectrosc. 85 (2012) 189.
[15] Spartan 08, Wavefunction Inc., Irvine, CA 92612, USA, 2008.
[16] M.J. Frisch, G.W. Trucks, H.B. Schlegel, G.E. Scuseria, M.A. Robb, J.R. Cheeseman, J.A. Montgomery, Jr., T. Vreven, K.N. Kudin, J.C. Burant, J.M. Millam, S.S. Iyengar, J. Tomasi, V. Barone, B. Mennucci, M. Cossi, G. Scalmani, N. Rega,G.A. Petersson, H. Nakatsuji, M. Hada, M. Ehara, K. Toyota, R. Fukuda, J. Asegawa, M. Ishida, T. Nakajima, Y. Honda, O. Kitao, H. Nakai, M. Klene, X. Li, J.E. Knox, H.P. Hratchian, J.B. Cross, C. Adamo, J. Jaramillo, R. Gomperts, R.E. Stratmann, O. Yazyev, A.J. Austin, R. Cammi, C. Pomelli, J.W. Ochterski, P.Y. Ayala, K. Morokuma, G.A. Voth, P. Salvador, J.J. Dannenberg, V.G. Zakrzewski, S. Dapprich, A.D. Daniels, M.C. Strain, O. Farkas, D.K. Malick, A. D. Rabuck, K. Raghavachari, J.B. Foresman, J.V.Ortiz, Q. Cui, A.G. Baboul, S. Clifford, J. Cioslowski, B.B. Stefanov, G. Liu, A.Liashenko, P. Piskorz, I. Komaromi, R.L. Martin, D.J. Fox, T. Keith, M.A. Al-Laham, C.Y. Peng, A. Nanayakkara, M. Challacombe, P.M.W. Gill, B. Johnson, W. Chen, M.W. Wong, C. Gonzalez, J.A. Pople, Gaussian 03, Revision E.01, Gaussian, Inc., Pittsburgh PA, 2003.
[17] H.B. Schlegel, J. Comput. Chem. 3 (1982) 214.
[18] G. Rauhut, P. Pulay, J. Phys. Chem. 99 (1995) 3093.
[19] D. Michalska, R. Wysokinski, Chem. Phys. Lett. 403 (2005) 211.
[20] Ö. Dereli, H. Cavusoglu, E. Turkkan, A. Ozmen, A. Ilik, Energy Educ. Sci. Technol. Part A. 28 (1) (2011) 485.
[21] M. Lutz, A.L. Spek, Acta Cryst. C61 (2005) 639.
[22] M.D. Halls, J. Velkovski, H.B. Schlegel, Theor. Chem. Acc. 105 (2001) 413.
[23] P. Pulay, G. Fogarasi, F. Pang, J.E. Boggs, J. Am. Chem. Soc. 101 (1979) 2550.
[24] J. Baker, A.A. Jarzecki, P. Pulay, J. Phys. Chem. A 102 (1998) 1412.
[25] O. Alver, C. Parlak, Vib. Spectrosc. 54 (2010) 1–9.
[26] Gauss View, Version 4.01, Dennington II, Roy, T. Keith, J. Millam, K. Eppinnett, W. L.Hovell, R. Gilliland, Semichem, Inc., Shawnee Mission, KS, 2003.
[27] G. Varsanyi, Assignments for vibrational spectra of seven hundred benzene derivatives, vols. 1–2, Adam Hilger, 1974.
[28] M. Jag, Organic Spectroscopy – Principles and Applications, second ed., Narosa Publishing House, New Delhi, 2001.
[29] N. Sundaraganesan, B. Anand, C. Meganathan, B.D. Joshua, Spectrochim. Acta A 68 (2007) 561.
[30] M.K. Subramanian, P.M. Anbarasan, S. Manimegalai, J. Raman Spectrosc. 40 (2009) 1657.
[31] V. Krishnakumar, N. Jayamani, R. Mathammal, K. Parasuraman, J. Raman Spectrosc. 40 (2009) 1551.
[32] P.J. O'Malley, J. Mol. Struct. Theochem. 755 (2005) 147.
[33] R.M. Silverstein, F.X. Webster, J. Kiemle, Spectrometric Identification of Organic Compounds, seventh ed., John Wiley & Sons, New York, 2005.
[34] J.H.S. Green, D.J. Harrison, W. Kynaston, Spectrochim. Acta 28 (1972) 33.
[35] S.N. Azizi, M.J. Chaichi, M. Yousefi, Spectrochim. Acta Part A 73 (2009) 101.
[36] I. Fleming, Frontier Orbitals and Organic Chemical Reactions, John Wiley and Sons, New York, 1976.
[37] J.S. Murray, Molecular Electrostatic Potentials, Concepts and Applications, Elsevier, Amsterdam, 1996.

[1] For interpretation of color in Figs. 1–7, the reader is referred to the web version of this article.

[38] J.M. Seminario, Recent Developments and Applications of Modern Density Functional Theory, vol. 4, Elsevier, 1999. pp. 800–806.

[39] T. Yesilkaynak, G. Binzet, F. Mehmet Emen, U. Florke, N. Kulcu, H. Arslan, Euro. J. Chem. 1 (2010) 1.